Collision avoidance trajectories for on-line trajectory optimization in C-arm CBCT

Sepideh Hatamikia[1,2], Ander Biguri[3], Gernot Kronreif[1], Tom Russ[4], Joachim Kettenbach[5], Wolfgang Birkfellner[2]

[1]Austrian Center for Medical Innovation and Technology, Wiener Neustadt, Austria
[2] Center for Medical Physics and Biomedical Engineering, Medical University of Vienna, Austria
[3] Institute of Nuclear Medicine, University College London
[4]Computer Assisted Clinical Medicine, Medical Faculty Mannheim, Heidelberg University, Germany
[5]Institute of Diagnostic and Interventional Radiology and Nuclear Medicine, Landesklinikum Wiener Neustadt, Austria

Abstract

Kinematic constraints due to the additional medical equipment or patient size are common while acquiring C-arm cone beam computed tomography (CBCT). Such constraints cause collisions with the imager while performing a full circular rotation and therefore eliminate the chance for three dimensional (3D) imaging in CBCT-based interventions. In a previous paper, we proposed a framework to develop patient-specific collision-free trajectories for the scenarios where circular CBCT is not possible. However, the proposed method required kinematic constraints to be known beforehand. As collisions are mainly unpredictable in the operation theater, a framework which enables a real-time trajectory optimization is of great clinical importance. In this study, we introduce a new search strategy which has the potential to optimize trajectories on-the-fly. We propose an optimization procedure which identifies trajectories with the highest information to reconstruct a Volume of Interest (VOI) by means of maximizing an objective function; then a local search is performed around the best selected initial candidates and better trajectory solutions are investigated among newly created neighbors. The experimental results based on two imaging targets inside an Alderson Rando phantom showed that proposed trajectories achieve image quality comparable to that of the reference circular CBCT while simulating strong kinematic constraints. The overall time required for the whole optimization process was around three to four minutes using one GPU.

1 Introduction

Recently, cone beam computed tomography (CBCT) has become an important imaging modality in interventional radiology [1, 2]. One important feature of interventional radiology is that a prior knowledge of patient anatomy (e.g. high quality CT or pre-operative CBCT) is usually available. This gives the opportunity to incorporate such prior knowledge into image acquisition process by using a customized CBCT. Nowadays, robotic CBCT C-arms enable additional degrees of freedom and extend the scanning geometry possibilities beyond the standard circular source-detector trajectories. Several studies have demonstrated an improvement in image quality and/or reduction the radiation dose using noncircular trajectories. In these studies, trajectory parameters were computed in the way to maximize the imaging performance of particular imaging tasks [3-5]. Gang et al. [3] proposed a target-based imaging acquisition framework for robotic C-arm CBCT systems using a gradient-based optimization of the tube current, reconstruction kernel and orbital tilt. Noncircular source-detector trajectories have been introduced using periodic and B-spline-based functions for simulation studies, as well as in neuroradiology applications to increase the image quality in a Volume of Interest (VOI) [4, 5].

Recently, optimal sinusoidal trajectories were proposed in order to avoid the metal parts of the imaged object while still assuring a high coverage in Radon space and its vicinity [6]. All the aforementioned researches [3-6] were effectively applied to C-arm CBCT trajectory optimization. However, in all these studies, hard constraints on the rotation angle were applied for the trajectory design; thus, the employed trajectories did not take patient-specific collisions into account. Furthermore, all these studies [3-6] calculated the optimal trajectory parameters in a (semi) offline manner.

In another study [7], patient-specific collision avoidance trajectories were proposed for linac-mounted CBCT devices using a virtual isocenter and variable magnification during data acquisition. Although their proposed trajectories could integrate case-specific collisions into the trajectory design, their method requires a high amount of computational time which hampers its usage for real-time trajectory optimization and therefore, it is not appropriate to react to unforeseen collisions which happen during interventions. To the best of our knowledge, the only study that introduced a real-time trajectory optimization was [8], in which the authors proposed optimizing the C-arm CBCT trajectories during the CBCT scan and performed the adjustments on-the-fly using a convolutional neural network and regressed an image quality measured over all possible next projections given the current X-ray image. However, the main focus of this research was metal artifact reduction and the trajectories introduced did not incorporate patient-specific collisions in their trajectory design. The research we present in this study is the first demonstration that proposes an on-the-fly trajectory optimization framework for customized CBCT acquisition that is able to react to scene-specific unforeseen collisions.

Our group has recently published a method to optimize imaging quality for CBCT using semi-circular scan trajectories which can also be arranged out-of-plane [9, 10]. A VOI is selected using a prior CT scan and a variety of possible trajectory combinations from short arcs is simulated while taking kinematic constraints into account. The optimal arc combination is designated based on the image quality within the VOI. The time needed for designing a patient specific trajectory was in the range of 80 minutes [9]. This required collisions and kinematic constraints to be known previously. As such constraints are mostly unpredictable in a clinical scenario, e.g. caused by additional medical devices or patient size (Fig. 1), a real time trajectory optimization protocol is of great clinical importance even at the cost of losing a bit of image quality.

In the current study, we introduce a search strategy to overcome the aforementioned computational constraints.

Compared to our previous study [9], the major scientific novelty of this study lies on the introduction of the new search strategy that enables the on-the-fly feature for the trajectory optimization scheme; this finally brings a remarkably important clinical benefit for interventions where a 3D CBCT is otherwise not possible due to unforeseen collisions.

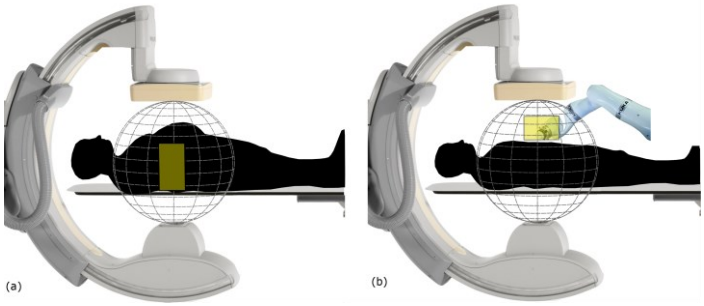

Figure 1. Two examples of common kinematic constraints during interventions. Collision due to the patient size (a), and due to other medical devices (b) [11].

2 Materials and Methods

2.A. Adaptation of workflow for the on-the-fly customized trajectory optimization

In this study, we modified our previous work to enable a dynamic optimization in the operation room which can integrate kinematic constraints emerging during the interventions into the trajectory optimization design.

We used the geometry of the Philips Allura FD20 Xper C-arm in order to define a set of possible arcs. The C-arm is able to perform two different types of rotations: 1) rotation by angle θ_1 towards the Right Anterior Oblique (RAO)/Left Anterior Oblique (LAO) direction while having a tilt ψ at various fixed Cranial (CRA)/Caudal (CAU) angles, 2) rotation by angle θ_2 towards the CRA/CAU direction while having a tilt φ at various fixed RAO/LAO angles. Different subset of arcs (each arc included around 80 projections) were defined similar to that in the previous work [9] (Fig 2. a, b). We simulated kinematic constraints as two forbidden areas on the geometry of the C-arm (represented as yellow rectangles in Fig. 2 c, d). The arcs which had more than 10% of their angular range in the two forbidden area were removed and those that had less than 10% in these areas were cropped (Fig. 2 e, f) [9]. In order to accelerate the optimization process in the current work, the previous approach was modified by sparsifying the initial subset of arcs (Fig. 2 e, f) to include just arcs for every six degrees (Fig. 2 g, h); this led to a significant reduction in the computation time. However, a reduction of the initial subset of arcs may introduce an unfavorable bias in the path selection process. To address this issue, we propose to perform a heuristic local search around the arcs with the largest amount of information. First, we selected the three arcs with the best objective function values as the arcs with highest amount of information. Then, we created new neighbor arcs for each of the three selected arcs and consequently, searched through such nearest neighbor arcs until an improvement in the objective function is observed. Finally, we selected the arc with the highest objective function value (Fig. 3). We repeated this procedure for the arc subsets RAO/LAO and CRA/CAU one after the other, with the previous best arcs were still being used, until a predefined number of arcs was designated as the final trajectory. We used the value of Feature SIMilarity Index (FSIM) as the objective function, as in our previous study. The pseudocode for this procedure is presented in Algorithm 1.

2.B. Image reconstruction

A modified version of the Tomographic Iterative GPU-based Reconstruction (TIGRE) toolkit [12] for arbitrary trajectories was used [9], but the Adaptive Steepest Descent Projection Onto Convex Sets (ASD-POCS) reconstruction was limited to five iterations. For simulations, we sampled projections every four degrees, and therefore, 20, 40, and 60 projections were simulated for trajectories that included one, two, and three arcs, respectively. Projection number reduction was done only in simulations for a further acceleration of the process; however, for the real data, the full sampling projections were used for reconstruction. For projection simulations, we used a monoenergetic forward model with added Poisson noise. Bare-beam fluence was also modeled to approximate device exposure.

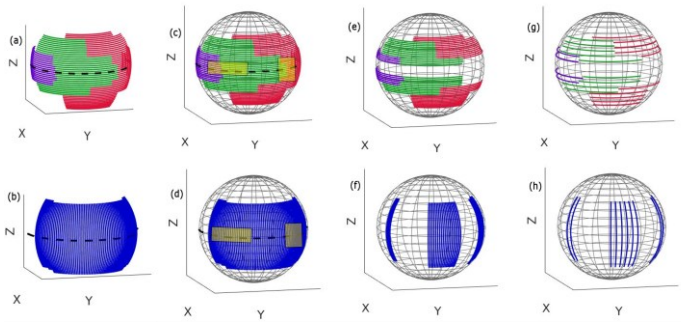

Figure 2. A) RAO/LAO arcs with CRA/CAU obliques shown in the purple, green, and red colors, (b) CRA/CAU arcs with RAO/LAO obliques shown in the blue color, (c) and (d) spherical plot of arcs with two forbidden areas, (e) and (f) spherical plot of the arcs after removing those that intersected the forbidden area, (g) and (h) spherical plot of these remaining arcs after sparsification. Only these arcs were in the search space for trajectory optimization. (Kinematic constraints are simulated as forbidden areas are shown as yellow rectangles) [11].

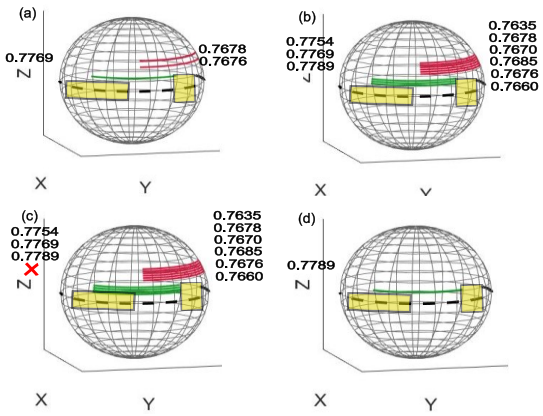

Figure 3. Illustration of the search strategy for optimizing the first best arc, (a) the three arcs with the highest objective function value are selected by searching through the RAO/LAO arc sparsely sampled initial subset (Fig. 2 g), (b-d) the nearby arcs are searched until the objective function decreased. The sign (×) shows that the arc included more than 10% of its angular range in the forbidden area, and therefore, was rejected from the search space and FSIM was not calculated.

Algorithm 1. Trajectory optimization

Input: Search space, number of desired arcs
Step 1: Simulate projections for all defined arcs with the digital phantom
Step 2: FOR 1: number of subsets
Step 3: FOR 1: number of arcs in subset

- Reconstruct the image using the set of projections related to the corresponding arc
- Crop the reconstructed image at the VOI
- Calculate the objective function at the cropped area

END
Step 4: Select best three arcs from Step3
Step 5: WHILE expanded arcs increase objective function
Step 6: FOR 1:number of arcs to expand

- Create neighboring arcs at one degree each side
- Evaluate objective function in newly created neighbors

END
END
Step 7: Select best arc and prepend to search space

2.B.1. Optimization of computational time

The implementation of ASD-POCS in the TIGRE toolbox was modified to remove CPU-GPU transfer functions and to run the reconstruction fully on the GPU. Our implementation takes approximately 1.4, 2.2, and 3.05 seconds for each ASD-POCS reconstruction (with five iterations), including 20, 40, and 60 projections using a computer with an NVIDIA GeForce RTX 2080 and a 32-core Advanced Micro Devices (AMD) processor. 256^3 voxel volumes with 512^2 projections were used for the reconstruction. The overall time required for the whole optimization process was around three to four minutes. The reported numbers in this study are using one GPU.

3 Results

In our experiments, two imaging targets in the thoracic spine (regions T3/T4 and T10/T11 for Target 1 and Target 2, respectively) of an Alderson-Rando phantom were evaluated. In the simulations, we optimized trajectories including three arcs for both imaging targets. 3D visualizations of the optimized trajectories compared to standard circular trajectory are shown in Fig. 4 a and Fig. 4 c for Target 1 and Target 2, respectively. The selected angular range and projection numbers related to optimized trajectories of both targets are shown in Table I. The (-) sign denotes rotation to the right/caudal directions and the (+) sign denotes rotation to the left/cranial. We implemented the optimal trajectories using a step-and-shoot protocol on C-arm to acquire real data. The reconstruction results were then compared to the C-arm circular trajectory (313 projections, 210° angular range). Furthermore, they were also compared with respect to a reconstruction from a partial circular trajectory with an angular range and projections equivalent to the optimized trajectory. Reconstruction results using simulation data as well as real data for the optimized trajectories, standard C- arm circular, and partial circular trajectories for both targets are shown in Fig 5. The reconstruction results were evaluated by FSIM and Universal Quality Image (UQI). For both indexes, the image quality metric between the prior CT and C-arm circular CBCT was considered the reference value. The quality index value between the prior CT and optimized/partial circular trajectory was also calculated as the measured value. The relative deviation between the reference and measured values was used for the image quality evaluation. According to the results of Table III, the optimized trajectories delivered relative deviations up to 9.47% and 4.06% in both image quality metrics for Target 1 and Target 2, respectively. A relative deviation up to 7.87% and 5.39% for Target 1 and Target 2, respectively, was also calculated for the reconstructed images related to partial circular trajectories. These results show a small decreased reconstruction performance (a slightly higher relative deviation) for Target 1, while a small increased image quality (a slightly lower relative deviation) for Target 2 for both image quality metrics when using optimized trajectories compared to the partial circular trajectory. However, the differences observed are not significant and reconstructed images from optimized trajectories revealed a comparable image quality for both targets with regard to the partial circular trajectories.

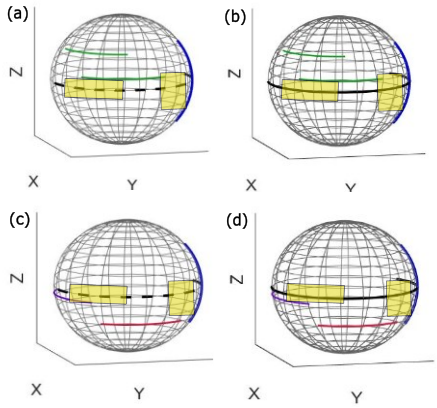

Figure 4. 3D visualization of the optimized trajectories (arcs shown in color) with respect to the C-arm circular trajectory (black dashed plot) and partial circular trajectory (black solid plot) for Target 1 (a, b) and Target 2 (c, d).

Table 1. The angular range and projection number of the three selected arcs for the optimized trajectories related to Target 1 and Target 2

Trajectory	Arc	Angle	Projection number per arc	Total number of projections
Target 1	Arc 1	θ_1= -39:1:+39, ψ= -26	72	**228**
	Arc 2	θ_2= -34:1:+40, φ= -60	75	
	Arc 3	θ_1= +44:1:+124, ψ=-6	81	
Target 2	Arc 1	θ_1= -22:1:+50, ψ= 10	73	**227**
	Arc 2	θ_2= -40:1:+38, φ= -50	79	
	Arc 3	θ_1= +9:1:+83, ψ=+32	75	

Table 1. Relative deviations (%) of image quality measures FSIM and UQI for Target 1 and Target 2 using both optimized and partial circular trajectories

Target	Image quality metric	Trajectory	Relative deviation (%)
Target 1	FSIM	Opt.	**9.47**
		Partial-circ.	**7.87**
	UQI	Opt.	**8.49**
		Partial-circ.	**4.83**
Target 2	FSIM	Opt.	**3.90**
		Partial-circ.	**5.39**
	UQI	Opt.	**4.06**
		Partial-circ.	**5.38**

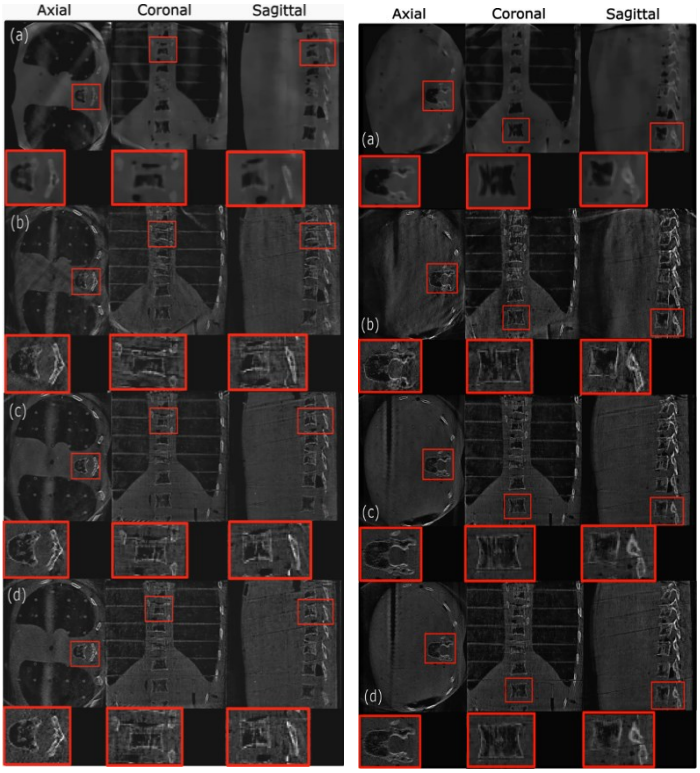

Figure 5. Reconstructions related to Target 1 (Left column) and Target 2 (Right column), (a) optimized trajectory based on simulation data, (b) optimized trajectory based on real data, (c) C-arm circular trajectory based on real data, and (d) partial circular trajectory based on real data. The display window has a range of 200-3000 HU for (a) and a range of 0-21 in gray values for (b-d), respectively.

4 Discussion and Conclusion

We proposed a framework for a patient-specific trajectory design for CBCT imaging which is suitable to react to unforeseen collisions. In fact, the major difference with the previous trajectory optimization approach [9] is that we now search for the optimal arcs within the most informative areas in 3D space to reconstruct the VOI (rather than searching among all plausible arcs as proposed in our previous study [9]), and consequently, we propose to perform a local search around the initially selected optimal arcs to find a better arc solution. Our results showed a slight decreased reconstruction performance for Target 1, while a small increase in image quality was seen for Target 2 using optimized trajectories compared to partial circular trajectories. Considering the fact that our approach is the first proposed protocol in literature that can facilitate CBCT for interventions in which a 3D circular CBCT would not be otherwise possible due to unpredictable collisions, our results show acceptable performance even if there is a slight reduction in the image quality for some targets compared to the partial circular trajectory. In this study, we achieved a considerably higher speed in comparison to our previous work [9], which required approximately 80 minutes for reconstruction. Our proposed trajectory optimization framework requires three to four minutes overall time on one GPU and a further reduction in time to about one minute is anticipated by using multiple GPUs. Our framework has the potential to be done on-the-fly; therefore, it can be considered suitable for interventions with unexpected and arbitrary collisions.

ACKNOWLEDGEMNET

This work was supported by ACMIT - Austrian Center for Medical Innovation and Technology, which is funded within the scope of the COMET program and funded by Austrian BMVIT and BMWFW and the governments of Lower Austria and Tyrol. We also gratefully acknowledge the support of NVIDIA Corporation for the donation of the Titan Xp GPU used for this research. The support from the personnel of the Institute of Diagnostic and Interventional Radiology and Nuclear Medicine, Wiener Neustadt, Austria, for the performance of measurements is also gratefully appreciated.

References

[1] R.C. Orth, R. J. Wallace, M.D. Kuo. “C-arm Cone-beam CT: General Principles and Technical Considerations for Use in Interventional Radiology”. Journal of Vascular and Interventional Radiology. 19. 6 (2008), pp. 814–820.

[2] S. Akpek. “Three-dimensional imaging and cone beam volume CT in C-arm angiography with flat panel detector”. Diagnostic and Interventional Radiology. 11. 1 (2005), pp. 10-30.

[3] G. J. Gang, J. W. Stayman, T. Ehtiati, J. H. Siewerdsen. “Task-driven image acquisition and reconstruction in cone-beam CT”. Physics in Medicine and Biology. 60.8 (2015), pp. 3129–3150.

[4] J. W. Stayman, S. Capostagno, G.J. Gang GJ, J. H. Siewerdsen. “Task-driven source–detector trajectories in cone-beam computed tomography: I. Theory and methods”. Journal of Medical Imaging. 6.2 (2019), pp. 025002.

[5] S. Capostagno, J. W. Stayman, M. Jacobson, T. Ehtiati, C.R. Weiss, J.H. Siewerdsen. “Task-driven source–detector trajectories in cone-beam computed tomography: II. Application to neuroradiology”. Journal of Medical Imaging. 6.2 (2019), pp. 025004.

[6] G.J. Gang, J.H. Siewerdsen, J.W. Stayman. “Non-circular CT orbit design for elimination of metal artifacts. In: Chen GH, Bosmans H (eds) Medical imaging 2020: physics of medical imaging”, vol 11312. International Society for Optics and Photon ics (SPIE), Bellingham, pp. 531–536. DOI:10.1117/12. 2550203.

[7] A. M. Davis, E.A. Pearson, X. Pan, C. H. A. Pelizzari, et al.. “Collision-avoiding imaging trajectories for linac mounted cone-beam CT”. Journal of X-Ray Science. 27. 2 (2019), pp 1-16.

[8] M. Thies, J.N. Zäch, C. Gao, R. Taylor, et al. “A learning-based method for online adjustment of C-arm Cone-beam CT source trajectories for artifact avoidance”. International Journal of Computer Assisted Radiology and Surgery. 15 (2020), pp. 1787–1796. DOI: 10.1007/s11548-020-02249-1.

[9] S. Hatamikia, A. Biguri, G. Kronreif, J. Kettenbach, et al. “Optimization for customized trajectories in Cone Beam Computed Tomography”. Medical Physics. 47. 10 (2020). DOI: 10.1002/mp.14403.

[10] S. Hatamikia, A. Biguri, G. Kronreif, et al. “CBCT reconstruction based on arbitrary trajectories using TIGRE software tool”, Proceeding of the 19th joint conference on new technologies for Computer/Robot Assisted Surgery (CRAS). March 2019, Genova, Italy.

[11] S. Hatamikia, A. Biguri, G. Kronreif, et al. “Toward on-the-fly trajectory optimization for C-arm CBCT under strong kinematic constraints”. Conditionally accepted in PLOS ONE journal on Jan 5th 2021.

[12] A. Biguri, M. Dosanjh, S. Hancock, M. Soleimani. “TIGRE: a MATLAB-GPU toolbox for CBCT image reconstruction”. Biomedical Physics & Engineering Express. 2 (2016), pp. 055010.